

**Microwave-assisted deep eutectic solvent synthesis of Sr-doped
LaNiO₃-derived Ni-based oxides for efficient NH₃ decomposition**

Yu-Long Duan ^a, Jun-Ying Yu ^a, Zhen Chen ^{a*}, Li Yang ^{a*}, Yuan-Hang Qin ^{a, b*},

Tielin Wang ^a, Cun-Wen Wang ^a

^a Key Laboratory for Green Chemical Process of Ministry of Education, Hubei Key Lab of Novel Reaction & Green Chemical Technology, School of Chemical Engineering and Pharmacy, Wuhan Institute of Technology, Wuhan 430205, China.

^b Joint Laboratory of Catalytic Materials and Engineering, School of Chemical Engineering and Pharmacy, Wuhan Institute of Technology, Wuhan 430205, China.

*Corresponding author. Tel & Fax: +86-27-87194882. E-mail: qyhsir@qq.com, yhqin@wit.edu.cn (Y.-H. Qin); zhende_888@126.com (Z. Chen); liyang@wit.edu.cn (L. Yang).

Physical characterization

The crystal structure of catalyst was characterized by X-ray diffraction (XRD, D8 Advance, Bruker). The morphology of catalyst was analyzed using scanning electron microscopy (SEM, S-4800, Hitachi) and high-resolution transmission electron microscopy (HRTEM), high-angle annular dark field scanning transmission electron microscopy (HAADF-STEM), and energy dispersive X-ray spectroscopy (EDS) (JEM-2100F, JEOL). The textural property of catalyst was characterized by N₂ sorption (Autosorb IQ-MP-MP). The reducibility and alkalinity of catalyst were characterized by hydrogen temperature programmed reduction (H₂-TPR) and CO₂ temperature programmed desorption (CO₂-TPD) (ChemStar, Quanta chrome Instruments), respectively. The surface information of catalyst was obtained using X-ray photoelectron spectrometry (XPS, Escalab 250Xi, Thermo Scientific). In-situ diffuse reflectance infrared Fourier transform spectroscopy (in-situ DRIFTS) measurements were conducted on a Nicolet iS50 spectrometer (Thermo Scientific).

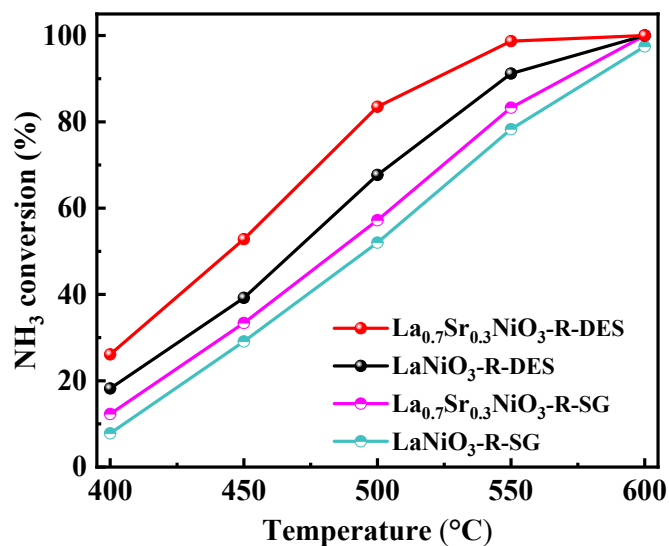


Fig. S1. Temperature-dependent NH₃ decomposition performance of LaNiO₃-R and La_{0.7}Sr_{0.3}NiO₃-R synthesized by the microwave-assisted DES and SG methods at a WHSV of 30,000 mL·g_{cat}⁻¹·h⁻¹.

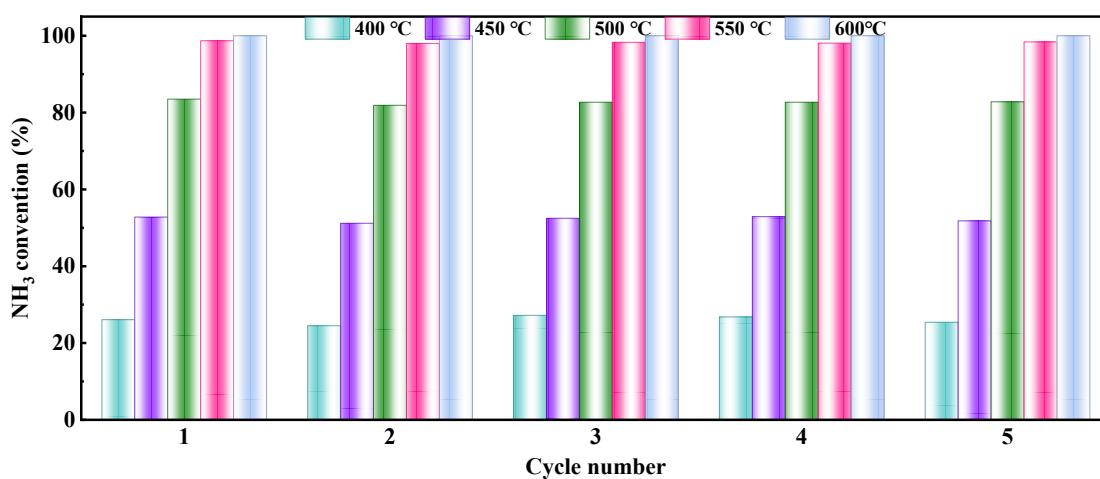


Fig. S2. The cyclic stability test of La_{0.7}Sr_{0.3}NiO₃-R catalyst (400–600 °C, WHSV = 30,000 mL·g_{cat}⁻¹·h⁻¹).

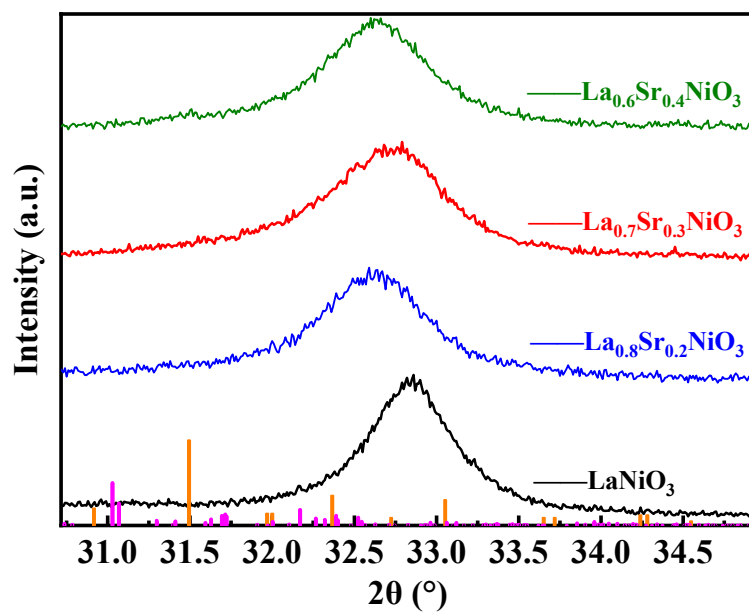


Fig. S3. Enlarged XRD patterns of $\text{La}_x\text{Sr}_{1-x}\text{NiO}_3$ catalysts.

Table S1. Textural properties of $\text{La}_x\text{Sr}_{1-x}\text{NiO}_3$ and $\text{La}_x\text{Sr}_{1-x}\text{NiO}_3\text{-R}$.

Sample	S_{BET} ($\text{m}^2\cdot\text{g}^{-1}$)	V_{T} ($\text{cm}^3\cdot\text{g}^{-1}$)	Pore size (nm)
LaNiO_3	28	0.19	16
$\text{La}_{0.8}\text{Sr}_{0.2}\text{NiO}_3$	31	0.24	32
$\text{La}_{0.7}\text{Sr}_{0.3}\text{NiO}_3$	22	0.12	24
$\text{La}_{0.6}\text{Sr}_{0.4}\text{NiO}_3$	20	0.13	25
$\text{LaNiO}_3\text{-R}$	27	0.15	22
$\text{La}_{0.8}\text{Sr}_{0.2}\text{NiO}_3\text{-R}$	36	0.15	17
$\text{La}_{0.7}\text{Sr}_{0.3}\text{NiO}_3\text{-R}$	33	0.19	23
$\text{La}_{0.6}\text{Sr}_{0.4}\text{NiO}_3\text{-R}$	22	0.16	29

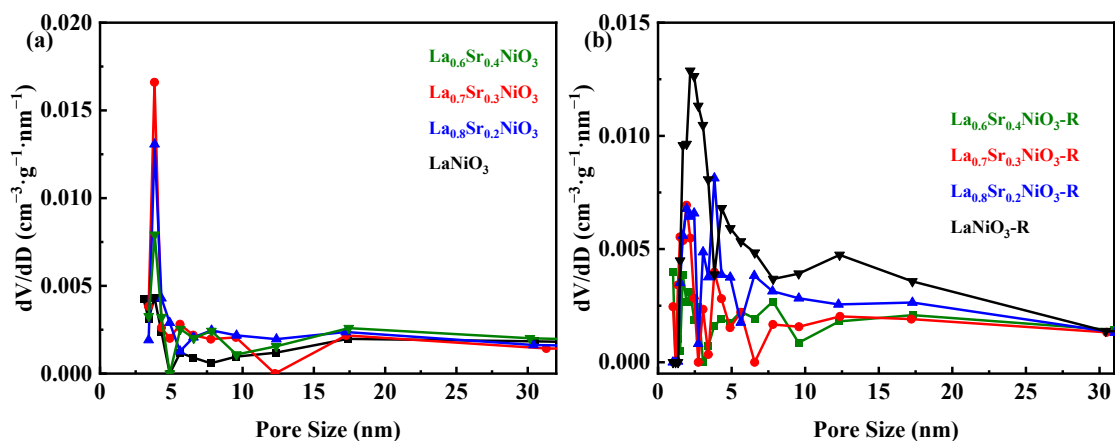


Fig. S4. Pore size distribution curves of $\text{La}_x\text{Sr}_{1-x}\text{NiO}_3$ (a) and $\text{La}_x\text{Sr}_{1-x}\text{NiO}_3\text{-R}$ catalysts (b).

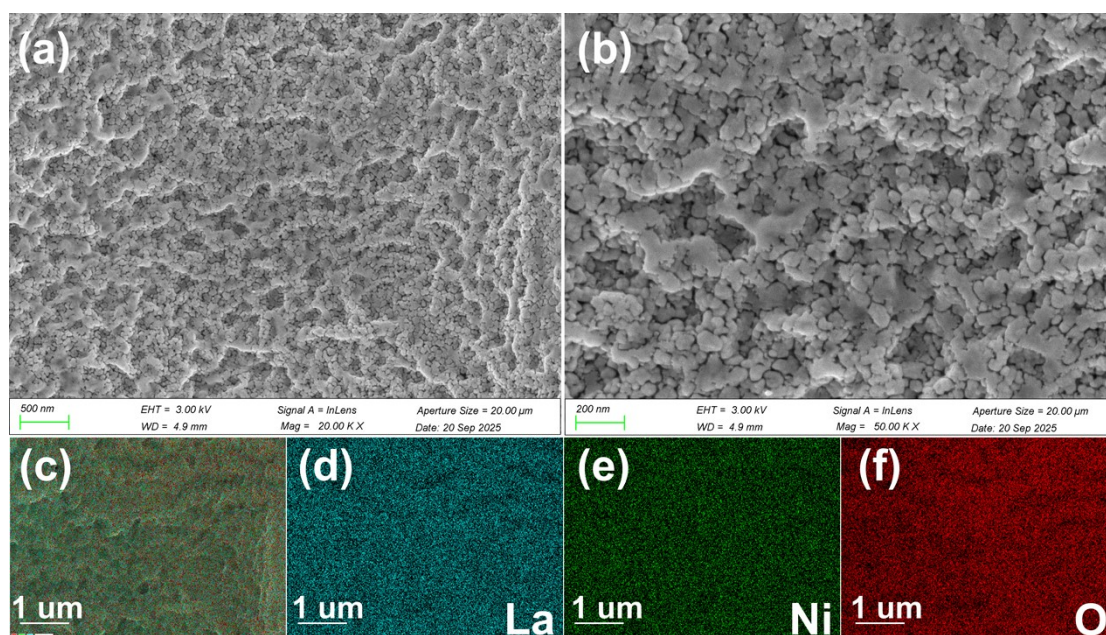


Fig. S5. SEM images of the LaNiO_3 catalyst at different magnifications: (a) $20,000\times$ and (b) $50,000\times$, and the corresponding EDS elemental mapping images showing the distribution of (c) all detected elements, (d) O, (e) Ni, and (f) La.

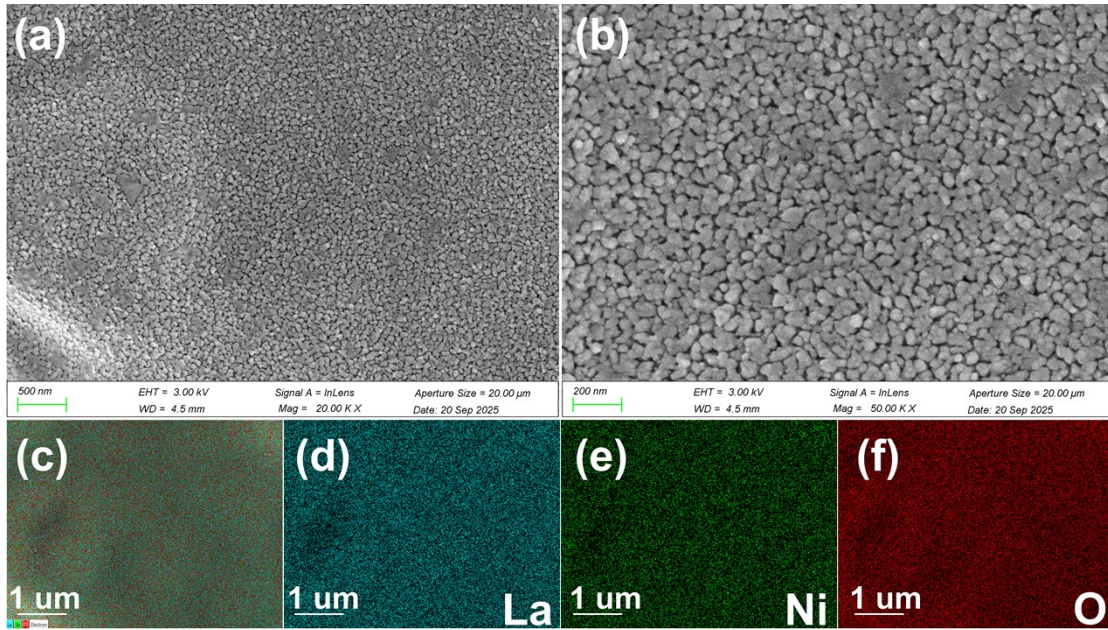


Fig. S6. SEM images of the $\text{LaNiO}_3\text{-R}$ catalyst at different magnifications: (a) $20,000\times$ and (b) $50,000\times$, and the corresponding EDS elemental mapping images showing the distribution of (c) all detected elements, (d) O, (e) Ni, and (f) La.

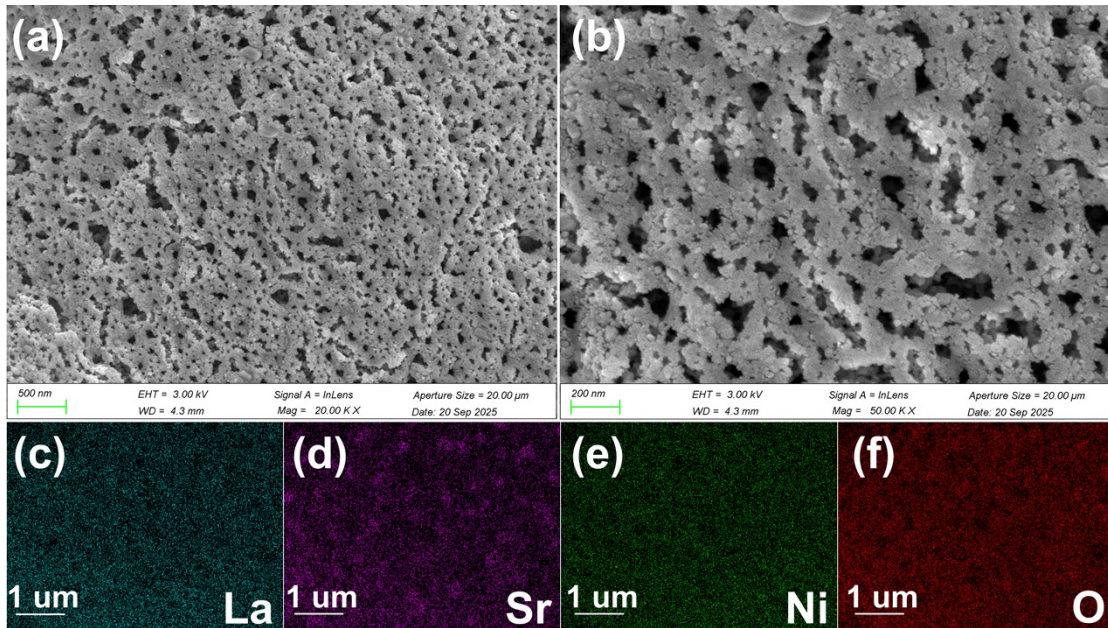


Fig. S7. SEM images of the $\text{La}_{0.7}\text{Sr}_{0.3}\text{NiO}_3$ catalyst at different magnifications: (a) $20,000\times$ and (b) $50,000\times$, and the corresponding EDS elemental mapping images showing the distribution of (c) Sr, (d) O, (e) Ni, and (f) La.

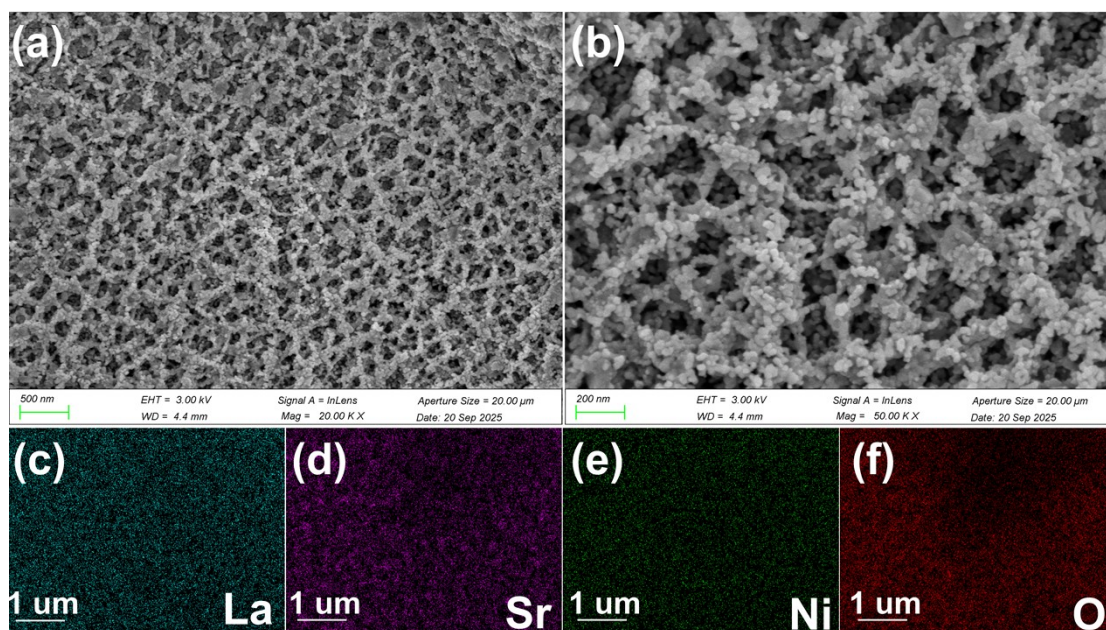


Fig. S8. SEM images of the $\text{La}_{0.7}\text{Sr}_{0.3}\text{NiO}_3\text{-R}$ catalyst at different magnifications: (a) 20,000 \times and (b) 50,000 \times , and the corresponding EDS elemental mapping images showing the distribution of (c) Sr, (d) O, (e) Ni, and (f) La.

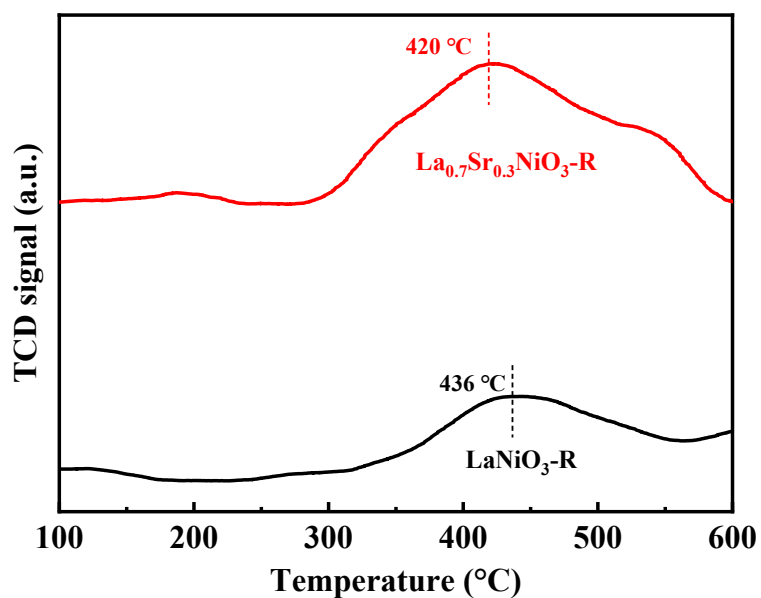


Fig. S9. N_2 -TPD results for $\text{LaNiO}_3\text{-R}$ and $\text{La}_{0.7}\text{Sr}_{0.3}\text{NiO}_3\text{-R}$ catalysts.

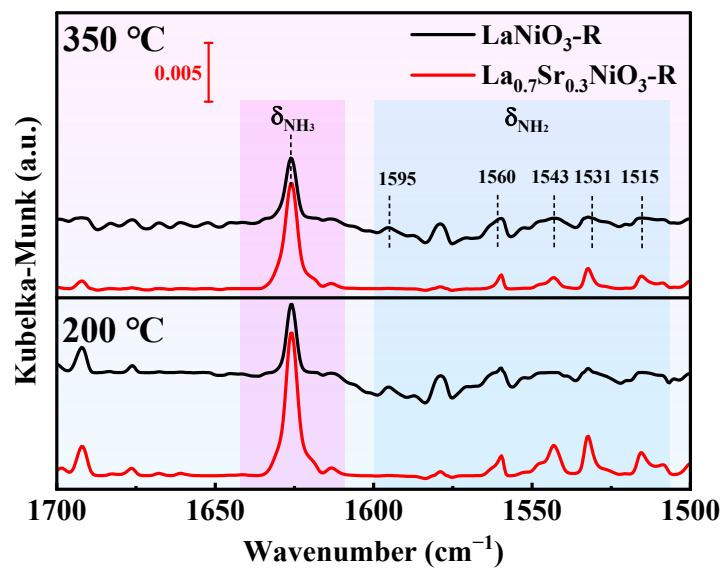


Fig. S10. Comparison of the in situ DRIFTS spectra of LaNiO₃-R and La_{0.7}Sr_{0.3}NiO₃-R catalysts at 200 and 350 °C.